Enhancement of jaw bone regeneration via ERK1/2 activation using dedifferentiated fat cells

Seiichi Fujisaki[1,2], Hiroshi Kajiya[1,3*], Tsukasa Yanagi[2], Munehisa Maeshiba[1,2], Kae Kakura[2], Hirofumi Kido[2] and Jun Ohno[1]

[1]Oral Medicine Research Center, Fukuoka Dental College, 2-15-1Tamura, Fukuoka, Japan

[2] Department of Oral Rehabilitation, Fukuoka Dental College, 2-15-1Tamura, Fukuoka, Japan

[3]Department of Physiological Science and Molecular Biology, Fukuoka Dental College, 2-15-1Tamura, Fukuoka, Japan

Short Title: Jaw bone regeneration with DFAT cells

***Corresponding author**

Department of Physiological Science and Molecular Biology, Fukuoka Dental College, Fukuoka, 8140193 Japan

E-mail address: kajiya@college.fdcnet.ac.jp

Competing interests

The authors declare that they have no competing interests.

Abstract

Purpose: Mesenchymal stem/stromal cells (MSCs) are multipotent and self-renewing cells that are extensively used in tissue engineering. Adipose tissues are known to be the sources of two types of MSCs, namely adipose tissue–derived MSCs (ASCs) and dedifferentiated fat (DFAT) cells. Although ASCs are sometimes transplanted for clinical cytotherapy, the effects of DFAT cell transplantation on mandibular bone healing remain unclear.

Methods: We assessed whether DFAT cells have osteogenerative potential compared with ASCs in rats in vitro. In addition, to elucidate the ability of DFAT cells to regenerate the jaw bone, we examined the effects of DFAT cells on new bone formation in a mandibular defect model in a) 30-week-old rats and b) ovariectomy-induced osteoporotic rats in vivo.

Results: Osteoblast differentiation with bone morphogenetic protein-2 (BMP-2) or osteogenesis-induced medium upregulated the osteogenesis-related molecules in DFAT cells compared with in ASCs. BMP-2 activated the phosphorylation signaling pathways of ERK1/2 and Smad2 in DFAT cells, but minor Smad1/5/9 activation was noted in ASCs. The transplantation of DFAT cells into normal or ovariectomy-induced osteoporotic rats with mandibular defects promoted new bone formation compared with that of ASCs.

Conclusion: DFAT cells promoted osteoblast differentiation and new bone formation through ERK1/2 and Smad2 signaling pathways in vitro. The transplantation of DFAT cells promoted new mandibular bone formation in vivo compared with that of ASCs. These results suggest that transplantation of ERK1/2-activated DFAT cells shorten the mandibular bone healing process in cytotherapy.

Key words: Bone regeneration, Dedifferentiated fat cells, Adipose tissue–derived mesenchymal stem/stromal cells, Cell transplantation, Mandibular defect

Introduction

Mesenchymal stem/stromal cells (MSCs) are multipotent somatic stem cells that can differentiate into various mesodermal cells, such as osteoblasts, chondrocytes, myocytes, and adipocytes [1]. MSCs are isolated from bone marrow as well as other connective tissues, such as adipose tissue, periosteum, synovium, and deciduous teeth [2]. MSCs represent unique opportunities in cellular regeneration therapy owing to their ability to stimulate the regeneration of damaged tissues and organs. MSC transplantation has already been applied in several clinical trials, such as in fracture nonunion, osteogenesis imperfecta, posterior spinal fusion, distraction osteogenesis, and osteoarthritis [3, 4]. However, the proliferative and differentiation capacities of MSCs are reduced according to the age and disease state of the host recipients [5]. Furthermore, MSC transplantations in patients with bone diseases, such as osteoporosis, rheumatoid arthritis, and osteoarthritis, have been reported to exhibit low proliferative and differentiation capacities [6, 7]. Alternative types of stem/stromal cells are needed for cellular therapy. This new type of stem cells is required given that these cells can be isolated easily at large amounts form targeted connective tissues from elderly patients and patients with bone disease.

Adipose tissues are abundant in the entire body and are known to contain two types of

stem/stromal cells, namely adipose tissue–derived MSCs (ASCs) and dedifferentiated fat (DFAT) cells [8, 9]. DFAT cells have been reported to be a highly homogeneous and proliferative cell population and have a multilineage potential for differentiation into mesenchymal tissue lineages in appropriate culture conditions [10–13].

Transplantation of DFAT cells into injured tissues have been reported to contribute to regeneration of some damaged tissues [11, 13–15]. Because DFAT cells can be obtained and expanded from small amounts of subcutaneous adipose tissues, regardless of age and disease type, DFAT cells could potentially be used in autologous cell-based therapies including patients with metabolic disorders. However, it is still unclear whether DFAT cells contribute to bone regeneration in patients with metabolic bone diseases in vivo, especially in cytotherapy cases.

The aim of present study was to assess whether the osteogenerative potential, including that in the activation of signaling pathways, of DFAT cells in vitro is higher than that of ASCs. In addition, to elucidate the ability of DFAT cells to regenerate bone in normal patients and patients with osteoporosis, we examined the effects of transplantation of DFAT cells on new bone regeneration in a mandibular bone defect model in normal and ovariectomy-induced (OVX) rats in vivo.

Materials and Methods

Isolation and cultures of ASCs

All animals were used in accordance with National Institutes of Health guidelines, and the Animal Care Committee of the Fukuoka Dental College (Fukuoka, Japan) approved protocol (Certification Nos. 17004 and 18004).

To isolate ASCs and adipocytes from abdominal adipose tissue, we performed the following protocol. Approximately 1 g of abdominal adipose tissue was collected from male rat (age, 24–30 weeks; Kyudo Co., Tosu, Japan). The tissue was minced into fine pieces and digested with 0.1% collagenase solution (Collagenase Type I; Koken Co., Ltd., Tokyo, Japan) in a container at 37°C for 1 h. After centrifugation at 1,400 rpm for 3 min, the precipitate was collected as stromal vascular fraction including ASCs. ASCs were cultured with Dulbecco's Modified Eagle's Medium (DMEM; Fuji Film Wako, Japan) that contained 20% fetal bovine serum (Sigma–Aldrich Co., St. Louis, MO, USA). After 80% confluence was attained, the cells were cultured in DMEM with or without supplementation with BMP-2 (20 ng/ml, Pepro Tech. Inc., NJ, USA) or osteogenesis-induced medium (OIM) with β-glycerophosphate (10 mM, Sigma) and ascorbic acid (50 μg/mL, Sigma).

Isolation and ceiling cultures of DFAT cells

In parallel preparation, after the digested adipose tissue was centrifugated at 100 g for 1

min, the floating top layer that contained isolated mature adipocytes was collected. Approximately three drops of mature adipocytes were dropped into the culture medium. The cells floated and attached on the top surface inside the top part of the flask. After 7 days, the medium was removed and the flask was turned upside down so that the cells faced the bottom side. The cells were used for experiments before they reached passage 5. After 80% confluence was attained, the cells were cultured in DMEM with or without BMP-2 or OIM. In some experiments, the ASCs and DFAT cells were cultured with BMP-2 in the presence or absence of U0126.

RNA isolation and quantitative reverse transcription polymerase chain reaction

Total RNA was extracted from the cells using the TRIzol reagent. First-strand complementary deoxyribonucleic acid (cDNA) was synthesized from 3 μg total RNA using Super Script II reverse transcriptase according to the manufacturer's instructions (Invitrogen Carlsbad, CA, USA). To detect mRNA expression, we selected specific primers based on the nucleotide sequence of the resultant cDNA. Relative messenger RNA (mRNA) expression was normalized as the ratio of targeted mRNAs to β-actin expression levels.

Western blot analyses

Cells were lysed in TNT [0.1 M Tris-HCl (pH, 7.5), 0.15 M NaCl, 0.05% Tween-20; Roche, Basel, Switzerland] buffer. The protein content was measured with a protein assay kit (Pierce, Hercules, CA, USA). Then, 20 μg of each protein were subjected to 12.5% sodium dodecyl sulfate polyacrylamide gel electrophoresis, and the separated proteins were electrophoretically transferred to a polyvinylidene fluoride membrane at 75 V and 4°C for 1.5 h. The membrane was incubated with the antibodies against ALP, Runx2, Osterix (OSX), p-Smad1/5, p-Smad2, p-ERK1/2, Smad1/5, Smad2/3, ERK1/2, YY1 (Cell Signaling Technology, Tokyo, Japan), and β-actin (Sigma–Aldrich Co.) diluted (1:500) in 5% skimmed milk Tris-buffered saline with Tween 20 (TBST; 10 mM Tris-HCl, 50 mM NaCl, 0.25% Tween-20) plus 0.01% azide overnight at 4°C. The blots were washed in TBST and incubated for 1 h with horseradish peroxidase conjugated antirabbit or anti-mouse immunoglobulin-G secondary antibodies. The antibodies were diluted (1:2000) in 5% skimmed milk TBST and were developed using an enhanced chemiluminescent system (GE Healthcare, Tokyo, Japan).

Flow cytometry analyses

Fluorescence-activated cell sorting (FACS) was performed to characterize the ASCs and

DFAT cells. The following antibodies conjugated with fluorescein isothiocyanate (FITC) or phycoerythrin (PE) were used as MSC markers: anti-CD29-PE, anti-CD44-FITC, anti-CD90-PE, and mouse IgGa1 isotype control (BD Bioscience, CA, USA). The labeled cells were analyzed by flow cytometry using the On-chip system (On-chip Biotechnologies Co., Ltd., Tokyo, Japan). The ratio of each antibody-positive cell to the total cells was quantified using the associated analysis software. In some experiments, marker-positive MSCs were sorted and collected using FACS.

Alizarin red staining

After culturing with or without OIM, the cells were washed twice with phosphate-buffered saline and fixed in 4% paraformaldehyde for 10 min. The cells were then stained with 1% alizarin red solution for 5 min. To quantify alizarin red staining, the stained cells were lysed in 5% formic acid at room temperature for 10 mins. The cell lysates were then collected and quantified using plate reader at an absorbance of 405 nm (ARVO MX, Perkin Elmer, MA, USA).

Transplantation of cells into mandibular bone defect model in normal rats and ovariectomy (OVX) rats

The normal (30-week-old male Sprague–Dawley rats) and OVX rats (12-week-old male Sprague–Dawley rats) were likely to use as each type of model for low-turnover and high-turnover in bone metabolism. Thirty-week-old rats were anesthetized by inhaling isoflurane (Escaine, Pfizer, USA). After the onset of anesthesia, the area around the mandible was shaved and disinfected with 70% ethanol. A single incision was made on the skin, the internal muscle was peeled off, and a bone defect model was prepared with a 5-mm trephine bar after the mandibular body was clearly marked. Three groups were studied: a) control group (n =4) with 5-mm collagen sponges after bone defect preparation, b) ASC transplantation group (n = 5) with collagen sponges coated with ASC cells, and c) DFAT cell transplantation group (n = 5) with collagen sponges coated with DFAT cells.

In parallel experiments, ovariectomy (OVX) was performed on female Sprague–Dawley rats (age, 8 weeks). After the onset of anesthesia with isoflurane, the area around the posterior lumbar spine was shaved and disinfected with 70% ethanol. A skin incision was made at bilateral abdomen, the muscles around both kidneys were incised in two small areas on the left and right, and the ovaries were extracted together with the fat. The junction with the uterus was ligated with mosquito forceps, sectioned, and excised. To confirm the presence of osteoporosis 1 month after the ovariectomy, the bone mineral densities of the femurs of the studied rats were measured. Cells were also transplanted in

OVX rats.

Microcomputed tomography analyses

Microcomputed tomography (μ-CT) images were acquired with in vivo μ-CT equipment (Skyscan-1176, Bruker, Belgium) at 50 kV and 500 mA. Each μ-CT slice had a thickness equal to 35 μm. The percentage of new bone formation in the bone defect area was calculated from each μ-CT image as the area of the newly formed bone/area of the original defect created by trephination in accordance with the procedures described in our previous manuscript [16]. First, the newly formed bone areas in the sagittal μ-CT images were quantified in two dimensions (2D) using WINROOF (Mitani Corporation, Tokyo, Japan). On each μ-CT image slice, 5-mm diameter circles were drawn for analyses. A series of 10 μ-CT images that showed the areas with the highest amounts of new bone formation were used for one sample analysis. The percentage of new bone formation in the defect (% of new bone) was calculated as the total area of new bone formed per 5 μ-CT images × 100.

Before measurements, images were adjusted so that the second molar was positioned in the vertical plane. Edited images were stored and analyzed using CT-An image analysis software (Bruker, Belgium). The section with the most complete view of the second molar and alveolar bone was used as the standard section, with 20 additional sections on the

buccal and lingual sides used to measure bone mineral density (BMD). The regions of alveolar bone surrounding the mesial and distal roots were analyzed. In some experiments, the BMD in bone surgical regions after transplantation were analyzed in two types of model rats with alveolar bone defects.

Hematoxylin and eosin (HE) staining

Rat alveolar bone were collected at 12 weeks after transplantation. The samples were fixed in 4% (w/v) paraformaldehyde/phosphate buffer (pH 7.4), decalcified with 0.24M ethylenediamine tetra-acetic acid solution, dehydrated with a graded alcohol series, cleared in xylene, and embedded in paraffin. Staining was performed using 3 μm-thick sections by routine procedures. The paraffin embedded sections were stained with HE to evaluate any histological changes. The border line between the new formed bones and old bones were evaluated the difference in the staining intensity of eosin (Supplemental file). All sections were histologically observed with a Nikon Eclipse fluorescence microscope (Nikon, Tokyo, Japan).

Statistical analyses

Data are expressed as the mean ± standard error of the mean (SEM). Differences were

analyzed using one-way analysis of variance and Scheffe's multiple comparison tests. P-values of <0.05 were considered significant.

Results

Osteogenesis-induced stimulation significantly upregulated the osteogenesis-related molecules in DFAT cells compared with ASCs

To characterize the ASCs and DFAT cells, FACS was first performed in the cells collected from the adipose tissues. Almost all ASCs (>80%) were positive for mesenchymal stem marker (CD40, CD90, and CD29; Figure 1A). In contrast, DFAT cells yielded the expressions of $CD40^+$ and $CD90^+$ markers (>80%), whereas the expressions of $CD29^+$ were <70% among all mesenchymal stem cell markers.

To clarify the ability of calcium deposition between ASCs and DFAT cells, both types of cells were cultured with OIM. The cells were fixed in 4% paraformaldehyde and then stained with alizarin red on days 0, 1, 3, 7, 14, and 21 after culture with osteogenesis stimulation. The intensity of alizarin red staining was increased on day 7 after osteogenesis induction in ASCs and on day 3 in the case of DFAT cells (Figure 1B). Furthermore, the intensity of alizarin red staining in DFAT cells significantly was stronger than that in ASCs on days 14 and 21 after osteogenesis-induced stimulation (Figure 1C).

Treatment with BMP-2 (20 ng/mL) increased the expression of osteogenesis-related genes, such as ALP, OSX, and Runx2 (mRNAs), compared with those in the control (without BMP-2) in both types of cells (Figure 2A). Furthermore, the mRNA expressions after BMP-2 treatment were significantly upregulated in DFAT cells in a time-dependent manner compared with that in ASCs. The mRNA expressions after BMP-2 treatment were noted on day 3 in ASCs and on day 1 in DFAT cells. Similar results were obtained after they were stimulated with OIM.

Both osteogenesis stimulations using OIM or BMP-2 also upregulated the expressions of osteogenesis-related molecules proteins, such as ALP, Runx2, and OSX, compared with those in control (only with DMEM) in both cell types (Figure 2B). The expressions of their proteins during osteogenesis stimulations were upregulated in dominant and time-dependent manners in DFAT cells compared with ASCs. Similar results were obtained in comparisons between the sorted $CD40^{+}/CD90^{+}$ DFAT cells and those of ASCs after BMP-2 treatment. The data indicated that DFAT cells were more potent in osteoblast differentiation than ASCs.

Furthermore, BMP-2 was upregulated greatly and activated its downstream molecules and the phosphorylation and expressions of Smad1/5 in ASCs. However, these effects were not noted in DFAT cells. In contrast, BMP-2 activated considerably the expression

and phosphorylation of ERK1/2 and Smad2 in DFAT cells, and their expressions were then increased significantly in DFAT cells compared with that in ASCs during osteogenesis (Figure 3A). Furthermore, to determine whether these transcription factors localize on the nucleus during osteogenesis in both types of cells, we examined the expressions of their molecules on nuclear proteins after BMP-2 treatment (Figure 3B). The translocation of p-ERK1/2 and p-Smad2, but not p-Smad1/5, increased significantly in DFAT cells compared with the corresponding expressions in ASCs.

To clarify whether ERK1/2 activation promotes osteogenesis, especially in DFAT cells, we examined the effects of U0126, an ERK1/2 inhibitor, on the expression of osteogenesis-related molecules in both types of cells in the present experiments.

As U1206 has mainly known to suppress the phosphorylation of ERK1/2 via the inhibition of catalytic activity of an upstream enzyme MEK1/2 [17], the incubation with U0126 in both type of cells decreased the expression of ERK1/2 mRNAs, phosphorylated ERK1/2 proteins, and total ERK1/2 proteins including phosphorylated and non-phosphorylated ERK1/2 proteins. The long incubation (7 days) may gradually be suppressed the phosphorylated ERK1/2 in early phase, and its continuous treatment completely suppressed their phosphorylation in late phase, suggesting in decrease in total amount of ERK1/2 proteins.

BMP-2 continually upregulated the expression of osteogenesis-related molecules, such as ALP, Runx2, and OSX, in the presence or absence of U0126 (10 μM) in ASCs. In contrast, the treatment of U0126 continually downregulated these molecules on day 1 and then slightly upregulated them in DFAT cells (compared with ASCs) after BMP-2 treatment (Figures 3C and 3D).

Transplantation with DFAT cells significantly promoted new bone formation in normal and OVX rats with mandibular defects

To clarify whether DFAT cells could potentiate new bone formation at a higher rate than ASCs in vitro, we transplanted a collagen sponge scaffold (control) with ASCs or DFAT cells into 30-week-old rats with a mandibular bone defect (Figures 4). Previous reports, including ours, have suggested that calvarial bone defects in rats >30 weeks old do not heal spontaneously during bone regeneration [16, 18]. Two weeks after transplantation, μ-CT images revealed no differences in the rat mandibular defects among the control, ASC transplantation, and DFAT cell transplantation groups. Twenty weeks after transplantation, new bone was formed around the defect in the rats transplanted with ASCs or DFAT cells at rates higher than those noted in the control groups (Figures 4A and 4B). Furthermore, the new bone formation significantly increased in the transplantation of DFAT cells compared with those of ASCs at 12 weeks after the

transplantation. However, there was no significant difference in BMD between DFAT transplantation and ASC transplantation on 12 weeks after surgery, suggesting that the bone in surgical regions may be osteoid with immature calcification. Consistent with the data that used μ-CT analysis, histological analysis of hematoxylin and eosin (HE)-stained sections showed that new bone regeneration increased in rats transplanted with DFAT cell compared with the levels of regeneration in the control or ASCs transplantation groups at 12 weeks after transplantation (Figure 4C).

Furthermore, to clarify the effect of cellular transplantation on mandibular bone healing in osteoporosis, we examined the cellular transplantation with or without ASC or DFAT cells in the mandibular defects of OVX rats (Figures 5A, 5C, and 5D). One month after OVX, the BMD was significantly decreased in mandibular bone of OVX rats compared with those of sham rats (Figure 5B). Two weeks after cell transplantation in OVX, μ-CT images revealed no differences in the rat mandibular defects among the control, ASCs transplantation, and DFAT cell transplantation groups (Figures 5A and 5C). Four weeks after transplantation, new bone in the ASC or DFAT cell-transplanted rats was formed at higher rates than those in the control rats. The increase in new bone formation and the BMD of DFAT-transplanted rats was approximately equal to that of ASC-transplanted rats at 12 weeks after transplantation (Figures 5C). Furthermore, the Consistent with the

μ-CT analysis data, histological analysis of HE-stained sections showed that the new bone regeneration increased in DFAT cell transplantation group at a rate higher than that in the control or ASCs transplantation group 12 weeks after transplantation (Figure 5D). The results indicated that the bone healing ability following transplantation with DFAT cells was slightly higher in normal rats with low-turnover in bone metabolism than that of ASCs and was approximately equal in OVX rats with high-turnover in bone metabolism . The results are suggesting that the therapeutic cytotherapy with transplantation of DFAT cells may be more effective on the patients with senile osteoporosis than that of postmenopausal osteoporosis.

Discussion

Bone regenerative therapy has been frequently performed for autografting. However, improvements are needed because of the increased impairment and infection in donors. Recently, the alternative cytotherapy using MSCs or somatic stem cells has been shown to be the most promising.

Adipose-derived stem cells have been classified as ASCs and DFAT cells. ASCs have been reported to be the potential source of stem cells and to be useful for cytotherapy [19, 20]. Although DFAT cells as well as ASCs have also been suggested as candidate MSCs

for cytotherapy, it is unclear whether the cells are useful and suitable for bone regeneration, especially in dental therapy for patients with metabolic bone diseases.

In the present study, we compared the potentials of osteoblast differentiation and new bone formation in DFAT cells and ASCs. We found that DFAT cells have a higher osteogenic differentiation potential and bone repair capacity than ASCs. Although the proliferation rates of DFAT cells were similar to those of ASCs, BMP-2 and OIM rapidly upregulated the expressions of osteogenesis-associated molecules, such as ALP, Runx2, and OSX in DFAT cells compared with ASCs. The ability of calcium deposition in DFAT cells was higher than that of ASCs, as demonstrated by alizarin red staining. Furthermore, the transplantation of DFAT cells promoted new bone formation in jaw bone defects in 30-week-old or OVX rats compared with that of ASCs. Therefore, DFAT cells have an advantage compared with ASCs in stem cells for cytotherapy because DFAT cells are more effective than ASCs.

The various TGF-β supper-families including BMP-2 has been well known are leading to ligand-specific modulation of the downstream signaling cascade at all cellular levels, such as Smad1/5/8 and smad2/3 complex [21]. BMPs have also been well known to induce canonical Smad1/5/9 phosphorylation [22]. It has been postulated that the p-Smad 1/5/9 pathways converge at the Runx2 gene and control the fate of critical bone formation

[23]. Additionally, OSX is indispensable for bone formation as it is required for the differentiation of preosteoblasts into mature osteoblasts [24]. In the present experiments, BMP-2 mainly activated the canonical pathway via Smad1/5 in ASCs. In contrast, we first found that BMP-2 greatly upregulated the phosphorylation of ERK1/2 and Smad2 in DFAT cells, a little effect in ASCs. The ERK/MAPK pathway was reported to regulate the osteoblast differentiation in MSCs and was associated with MAPK activity and Runx2 phosphorylation [25]. In contrast, the inhibition of ERK1/2 in ST2, a MSC line induced adipogenesis but led to decreased osteoblast differentiation. Furthermore, Runx2 has been reported to be regulated by ERK-dependent phosphorylation and has been shown to lead to increased transcriptional Runx2 activity [26]. In present experiments, a dominant activation of the ERK-Smad2 pathway of DFAT cells was documented compared with minor activation of ASCs.

DFAT cells have been reported to have a higher osteogenesis potential than ASCs following their transplantations in young rats [27, 28]. Both ASCs and DFAT cells have been well known to secrete several cytokines associated with bone formation, anti-inflammation, and angiogenesis [29, 30].There are some reports on differentiation of donor DFAT cells into mesodermal cells in recipient animals. Namely, the green fluorescent protein-labeled DFAT cells have been reported to be differentiated into

various cells including green fluorescent protein-positive cells, such as vascularized fat pads and smooth muscle [31, 32]. We found that the ability of osteoblastogenesis is higher in DFAT cells than in ASCs in the present in vitro experiments. Furthermore, new bone formation is likely to be induced in the edge of defect in present in vivo experiments, suggesting migration of the recipient osteoblast and/or DFAT cells and healing of the defect area.

DFAT cells have been reported to be isolated from donors regardless of age (range, 4–81 years) [10]. Furthermore, DFAT cells can also be prepared from patients with metabolic bone diseases, such as osteoporosis and rheumatoid arthritis. In the present experiments, BMP-2 can induce osteogenesis-related molecules in DFAT cells derived from elder fat tissues even though the rats were only 12 months old. Furthermore, the transplantation of DFAT cells formed new mandibular bone in more than 30-week-old and OVX-induced osteoporotic rats. These findings, together with the present study, suggest that DFAT cells can be used for autologous transplantation in patients at various ages, including elderly patients with or without metabolic bone diseases.

The homogenous ASCs have known to need a very large amount of adipose tissue for clinical therapy because ASCs are heterogeneous cell populations derived from stromal vascular fractions and typically include various types of cells [33, 34]. In contrast, DFAT

cells can be isolated from homogenous cells from a very small amount of adipose tissue because of dedifferentiated cells from pure mature adipocyte population. Highly homogenous DFAT cells can then be obtained through a less invasive surgical or liposuction procedure, thus leading to effects that are safer and more reproducible in clinical therapy. Although there are approaches that can be used to improve the tissue engineering efficiency using various MSCs, DFAT cells have advantages in optimal therapeutic protocols. These results suggest the need for alternative cell characteristics that can be easily prepared and expanded. Therefore, to achieve a more effective bone regenerative therapy, it is suggested that these patients must be transplanted with autologous DFAT cells in their constitutive active forms to induce ERK1/2-Smad2/3 signaling pathways.

Conclusion

DFAT cells greatly promoted osteoblast differentiation and calcium deposition in vitro compared with ASCs. DFAT cells also promoted new bone regeneration in normal or OVX-induced osteoporotic rats in vivo. These results indicate that transplantation of DFAT cells in cytotherapy leads to a shorter regenerative healing process, including new bone formation.

Acknowledgments

The authors would like to thank Dr. Kanno (Shimane University) for the technical guidance in mandibular bone defect rats. We also would like to thank Enago (Academic Proofreading Service; www.enago.jp) for the English language review.

This work was supported by Grants-in-Aid for Scientific Research from the Ministry of Education, Culture, Sports, Science and Technology of Japan (15K11062 to HK) and the Private University Research Branding Project of Fukuoka Dental College.

Author contributions

SF: performed the experiments and generated the data.

HK: conceived and designed the study, conducted the experiments, and wrote the manuscript.

TY: conducted the experiments and generated the data.

MM: conducted the experiments and generated the data.

KK: conducted the experiments and analyzed the data.

HK(Hirofumi Kido): designed the experiments and supervised the study.

JO: designed the experiments and supervised the study.

All authors have read and approved the final manuscript.

Ethics approval

Approval for the animal experiments was obtained from the Animal Care Committee of Fukuoka Dental College (protocol numbers: 17004 and 18004).

References

[1] Aldahmash A, Zaher W, Al-Nbaheen M, Kassem M. Human stromal (mesenchymal) stem cells: basic biology and current clinical use for tissue regeneration. Ann Saudi Med 2012;32:68-77. https://doi.org/10.5144/0256-4947.2012.68

[2] Wei X, Yang X, Han ZP, Qu FF, Shao L, Shi Y-F. Mesenchymal stem cells: a new trend for cell therapy. Acta Pharmacol Sin 2013;34:747-54. https://doi.org/ 10.1038/aps.2013.50.

[3] Takahashi K, Yamanaka S. Induction of pluripotent stem cells from mouse embryonic and adult fibroblast cultures by defined factors. Cell 2006;25;126:663-76. https://doi.org/ 10.1016/j.cell.2006.07.024

[4] Zhang ZY, Teoh SH, Hui JH, Fisk NM, Choolani M, Chan JK. The potential of human fetal mesenchymal stem cells for off-the-shelf bone tissue engineering application. Biomaterials 2012;33:2656-72 https://doi.org/ 10.1016/j.biomaterials.2011.12.025

[5] D'Ippolito G, Schiller PC, Ricordi C, Roos BA, Howard GA. Age-related osteogenic potential of mesenchymal stromal stem cells from human vertebral bone marrow. J Bone Miner Res 1999;14:1115-22. https://doi.org/ 10.1359/jbmr.1999.14.7.1115

[6] Jevotovsky DS, Alfonso AR, Einhorn TA, Chiu ES. Osteoarthritis and stem cell

therapy in humans: a systematic review. Osteoarthritis Cartilage. 2018;26:711-29. https://doi.org/ 10.1016/j.joca.2018.02.906

[7] Barry F. MSC Therapy for Osteoarthritis: An Unfinished Story.
J Orthop Res. 2019;37:1229-1235. https://doi: 10.1002/jor.24343.

[8] Yagi K, Kondo D, Okazaki Y, Kano K. A novel preadipocyte cell line established from mouse adult mature adipocytes. Biochem Biophys Res Commun 2004 3;321:967-74. https://doi.org/ 10.1016/j.bbrc.2004.07.055

[9] Kishimoto N , Honda Y, Momota Y, S Tran D. Dedifferentiated Fat (DFAT) cells: A cell source for oral and maxillofacial tissue engineering. Oral Dis 2018;24:1161-1167. https://doi.org/ 10.1111/odi.12832

[10] Matsumoto T, Mifune Y, Kawamoto A, Kuroda R, Shoji T, Iwasaki H et al. Fracture induced mobilization and incorporation of bone marrow-derived endothelial progenitor cells for bone healing. J Cell Physiol 2008;215:234-42. https://doi.org/ 10.1002/jcp.21309

[11] Sakuma T, Matsumoto T, Kano K, Fukuda N, Obinata D, Yamaguchi K, et al. Mature, adipocyte derived, dedifferentiated fat cells can differentiate into smooth muscle-like cells and contribute to bladder tissue regeneration. J Urol. 2009;182:355-65. https://doi.org/ 10.1016/j.juro.2009.02.103

[12] Kazama T, Fujie M, Endo T, Kano K. Mature adipocyte-derived dedifferentiated fat

cells can transdifferentiate into skeletal myocytes in vitro. Biochem Biophys Res Commun 2008;377:780-5.https://doi.org/ 10.1016/j.bbrc.2008.10.046

[13] Jumabay M, Matsumoto T, Yokoyama S, Kano K, Kusumi Y, Masuko T et al. Dedifferentiated fat cells convert to cardiomyocyte phenotype and repair infarcted cardiac tissue in rats. J Mol Cell Cardiol 2009;47:565-75. https://doi.org/ 10.1016/j.yjmcc.2009.08.004

[14] Obinata D, Matsumoto T, Ikado Y, Sakuma T, Kano K, Fukuda N et al. Transplantation of mature adipocyte-derived dedifferentiated fat (DFAT) cells improves urethral sphincter contractility in a rat model. Int J Urol 2011;18:827-34. https://doi.org/10.1111/j.1442-2042.2011.02865.x

[15] Sugawara A, Sato S. Application of dedifferentiated fat cells for periodontal tissue regeneration. Hum Cell 2014;27:12-21. https://doi.org/ 10.1007/s13577-013-0075-6

[16] Katsumata Y, Kajiya H, Okabe K, Fukushima T, Ikebe T. A salmon DNA scaffold promotes osteogenesis through activation of sodium-dependent phosphate cotransporters. Biochem Biophys Res Commun 2015;468:622-8. https://doi.org/ 10.1016/j.bbrc.2015.10.172

[17] Trappanese DM, Sivilich S, Ets HK, Kako F, Autieri MV, Moreland RS. Regulation of mitogen activated protein kinase by protein kinase C and mitogen-

activated protein kinase phosphatase-1 in vascular smooth muscle. Am J Physiol Cell Physiol. 2016;310:C921-30. https://doi: 10.1152/ajpcell.00311.2015.

[18] Levi B, Longaker TM. Concise review: adipose-derived stromal cells for skeletal regenerative medicine. Stem Cells 2011;29:576-82. https://doi.org/ 10.1002/stem.612

[19] Jeong JA, Ko KM, Bae S, Jeon CJ, Koh GY, Kim H. Genome-wide differential gene expression profiling of human bone marrow stromal cells. Stem Cells. 2007: 25:994-1002. https://doi: 10.1634/stemcells.2006-0604.

[20] Bougioukli S, Sugiyama O, Pannell W, Ortega B, Tan MH, Tang AH et al. Gene therapy for bone repair using human cells: Superior osteogenic potential of bone morphogenetic protein 2-transduced mesenchymal stem cells derived from adipose tissue compared to bone marrow. Hum Gene Ther 2018;29:507-519. https://doi.org/ 10.1089/hum.2017.097

[21] Nickel J and Mueller TD.Specification of BMP Signaling.

Cells 2019;8:1579. https://doi: 10.3390/cells8121579.

[22] Zhou Z, Xie J, Lee D, Liu Y, Jung J, Zhou L et al. Neogenin regulation of BMP-induced canonical Smad signaling and endochondral bone formation. Dev Cell 2010;19:90-102. https://doi.org/ 10.1016/j.devcel.2010.06.016

[23] Chen G, Deng C, Li YP. TGF-β and BMP signaling in osteoblast differentiation and bone formation. Int J Biol Sci 2012;8:272-88. https://doi.org/ 10.7150/ijbs.2929

[24] Zhang C. Transcriptional regulation of bone formation by the osteoblast-specific transcription factor Osx. J Orthop Surg Res 2010;5:37. https://doi.org/ 10.1186/1749-799X-5-37

[25] Li Y, Ge C, Franceschi RT. MAP Kinase-dependent RUNX2 phosphorylation is necessary for epigenetic modification of chromatin during osteoblast differentiation. J Cell Physiol. 2017;232:2427-2435. https://doi: 10.1002/jcp.25517.

[26] Ge C, Yang Q, Zhao G, Yu H, Kirkwood KL, Franceschi RT. Interactions between extracellular signal-regulated kinase 1/2 and p38 MAP kinase pathways in the control of RUNX2 phosphorylation and transcriptional activity. J Bone Miner Res 2012;27:538-51. https://doi.org/ 10.1002/jbmr.561

[27] Suzuki D, Akita D, Tsurumachi N, Kano K, Yamanaka K, Kaneko T, et al. Transplantation of mature adipocyte-derived dedifferentiated fat cells into three-wall defects in the rat periodontium induces tissue regeneration. J Oral Sci 2017;59:611-620. https://doi.org/ 10.2334/josnusd.16-0878

[28] Akita D, Kano K, Saito-TY, Mashimo T, Sato-S M, Tsurumachi N et al. Use of rat mature adipocyte-derived dedifferentiated fat cells as a cell source for periodontal tissue regeneration. Front Physiol 2016;7:50. https://doi.org/ 10.3389/fphys.2016.00050

[29] Kikuta S, Tanaka N, Kazama T, Kazama M, Kano K, Ryu J, et al. Osteogenic effects of dedifferentiated fat cell transplantation in rabbit models of bone defect and ovariectomy-induced osteoporosis. Tissue Eng Part A 2013;19:1792-802. https://doi.org/10.1089/ten.TEA.2012.0380

[30] Wu Y, Hoogduijn MJ, Baan CC, Korevaar SS, Kuiper R, Yan L et al. Adipose tissue-derived mesenchymal stem cells have a heterogenic cytokine secretion profile. Stem Cells Int. 2017;2017:4960831. https://doi.org/10.1155/2017/4960831.

[31] Nobusue H, Endo T, Kano K.
Establishment of a preadipocyte cell line derived from mature adipocytes of GFP transgenic mice and formation of adipose tissue.
Cell Tissue Res. 2008;332:435-446. https://doi.org/10.1007/s00441-008-0593-9.

[32] Obinata D, Matsumoto T, Ikado Y, Sakuma T, Kano K, Fukuda N et al. Transplantation of mature adipocyte-derived dedifferentiated fat (DFAT) cells improves urethral sphincter contractility in a rat model.

Int J Urol. 2011;18:827-834. https://doi.org/10.1111/j.1442-2042.2011.02865.x.

[33] Kishimoto N, Momota Y, Hashimoto Y, Ando K, Omasa T, Kotani J et al. Dedifferentiated fat cells differentiate into osteoblasts in titanium fiber mesh. Cytotechnology. 2013;65:15-22. https://doi.org/ 10.1007/s10616-012-9456-z

[34] Poloni A, Maurizi G, Leoni P, Serrani F, Mancini S, Frontini A et al. Human dedifferentiated adipocytes show similar properties to bone marrow-derived mesenchymal stem cells. Stem Cells. 2012 ;30:965-74. https://doi.org/ 10.1002/stem.1067

Figure legends

Fig 1. Flow cytometric analysis and representative images with alizarin red staining in adipose tissue–derived MSCs (ASCs) and dedifferentiated fat (DFAT) cells.

(A) Ratio of positive cells in CD44, CD29, and CD90 stemness markers in ASCs and DFAT cells. Mouse IgGa1was used as the control.

(B) Phase contrast images and alizarin red staining in ASCs and DFAT cells.

Scale bar = 200 μm. Alizarin red staining showed calcium deposition in bone morphogenetic protein-2 (BMP-2) treated ASC and DFAT cells. Scale bar = 5 μm.

(C) Calcium deposition rates were calculated at 14 and 21 weeks in alizarin red staining after OIM stimulation. Data shown are the means from four wells (mean ± SEM). Symbol ** denotes $p < 0.01$ in ASCs vs. DFAT cells.

Fig 2. Effects of osteogenesis stimulation with BMP-2 or osteogenesis-induced medium (OIM) on the expression of osteogenesis-related molecules in ASCs and DFAT cells.

(A) Cells were treated with or without BMP-2 on ASCs and DFAT cells. Expressions of osteogenesis-related genes ALP, OSX (Osterix), and Runx2 in both types of cells following BMP-2 (20 ng/mL) incubation. Samples were analyzed by quantitative

reverse transcription polymerase chain reaction (qRT-PCR), and were normalized to β-actin messenger ribonucleic acid (mRNA). Data shown are the means from six culture wells (mean ± standard error from the mean (SEM)). Symbols * and ** respectively indicate $p < 0.05$ and $p < 0.01$ in ASCs vs. DFAT cells.

(B) ASCs and DFAT cells were treated with BMP-2 (20 ng/mL) or OIM. Western blotting was conducted using targeted and β-actin antibodies in ASCs and DFAT cells. Similar results were obtained in four independent experiments.

Fig 3. BMP-2 dramatically activated the ERK1/2-Smad2/3 signaling pathway in DFAT cells, but only a minor activation was noted in ASCs.

(A) ASC and DFAT cells were treated with BMP-2 (20 ng/mL). Expressions of BMP receptor downstream signaling molecules, such as ERK1/2, Smad1/5, and Smad2/3, and their phosphorylated proteins following BMP-2 incubation. Samples were analyzed by Western blot analysis and normalized to β-actin proteins. Similar results were obtained in four independent experiments.

(B) ASCs and DFAT cells were treated with BMP-2 (20 ng/mL). Their nuclear proteins were collected from the total cellular proteins. Western blotting was conducted using targeted and β-actin antibodies in ASCs and DFAT cells. Similar results were obtained in three independent experiments.

(C) ASCs and DFAT cells were treated with BMP-2 in the presence or absence of U106 (10 μM), an ERK1/2 inhibitor. Expression of osteogenesis-related genes in both types

of cells following BMP-2 (20 ng/mL) incubation. Samples were analyzed by qRT-PCR and normalized to β-actin mRNA. Data shown are the means from six culture wells (mean ± SEM). Symbols * and ** respectively indicate $p < 0.05$ and $p < 0.01$ in ASCs vs. DFAT cells.

(D) ASCs and DFAT cells were treated with BMP-2 in the presence or absence of U106. Western blotting was conducted using targeted and β-actin antibodies in ASCs and DFAT cells. Similar results were obtained in three independent experiments.

Fig. 4. Transplantation with DFAT cells promoted new mandibular bone formation in normal rats.

(A) Sagittal microcomputed tomography (μ-CT) images of two types of cells transplanted at 2, 4, 8, and 12 weeks after mandibular bone surgery in rats (40 weeks old). The images on the left represent collagen sponge scaffold (control) transplantations, the central images represent the collagen sponge scaffold with ASCs transplantations, and the images on the right represent the collagen sponge scaffold with DFAT cell transplantations. The white dashed circles indicate mandibular bone defects (5 mm in diameter).

(B) Calculated new bone deposition rates at 2, 4, 8, and 12 weeks after mandibular bone surgery. The percentage of new bone mineral deposition was calculated from the bony tissue in the white dashed line in three types of grafting rats. Bone mineral density was calculated in the surgical regions (white dashed circles) at 12weeks after each transplantation. Data shown are the means from five rats (mean ± SEM). Symbol * denotes $p < 0.05$, and ** denotes $p < 0.01$ in control (day 0) vs. each transplantation group and in ASCs vs. DFAT cells at 12 weeks. (C) Schema of the location in

mandibular defects in 30-week-old rats. Histological coronal images of mandibular bone tissues at 12 weeks after the surgery. Symbols B and N indicate the original and new bones, respectively, and C indicates connective tissues. Scale bar = 500 μm.

Fig 5. Transplantation with DFAT cells promotes new mandibular bone regeneration in ovariectomy (OVX) rats. (A) Sagittal microcomputer tomography (μ-CT) images of two types of cells transplanted at 2, 4, 8, and 12 weeks after mandibular bone surgery in OVX rats. The white dashed circles indicate mandibular defects observed just after the surgery (5 mm in diameter). (B) Confirmation of decreased bone mineral density of mandibular bone in OVX and sham operation 1 month after ovariectomy in female rats (8 weeks old). The white dashed squares indicate measured areas in bone mineral density (C) Calculated new bone deposition rated at 2, 4, 8, and 12 weeks after transplantations. The percentage of new bone mineral deposition was calculated from the bony tissue in the white dashed line in three types of grafting rats. Data shown are the means from five rats (mean ± SEM). Symbol ** denotes $p < 0.01$ control vs. each transplantation group. Bone mineral density was calculated in the surgical regions (white dashed circles) at 12weeks after each transplantation. (D) Histological coronal images of mandibular tissues 12 weeks after surgery. Symbols B and N indicate the original and new bones, respectively, and C indicates connective tissues. Scale bar = 500 μm.

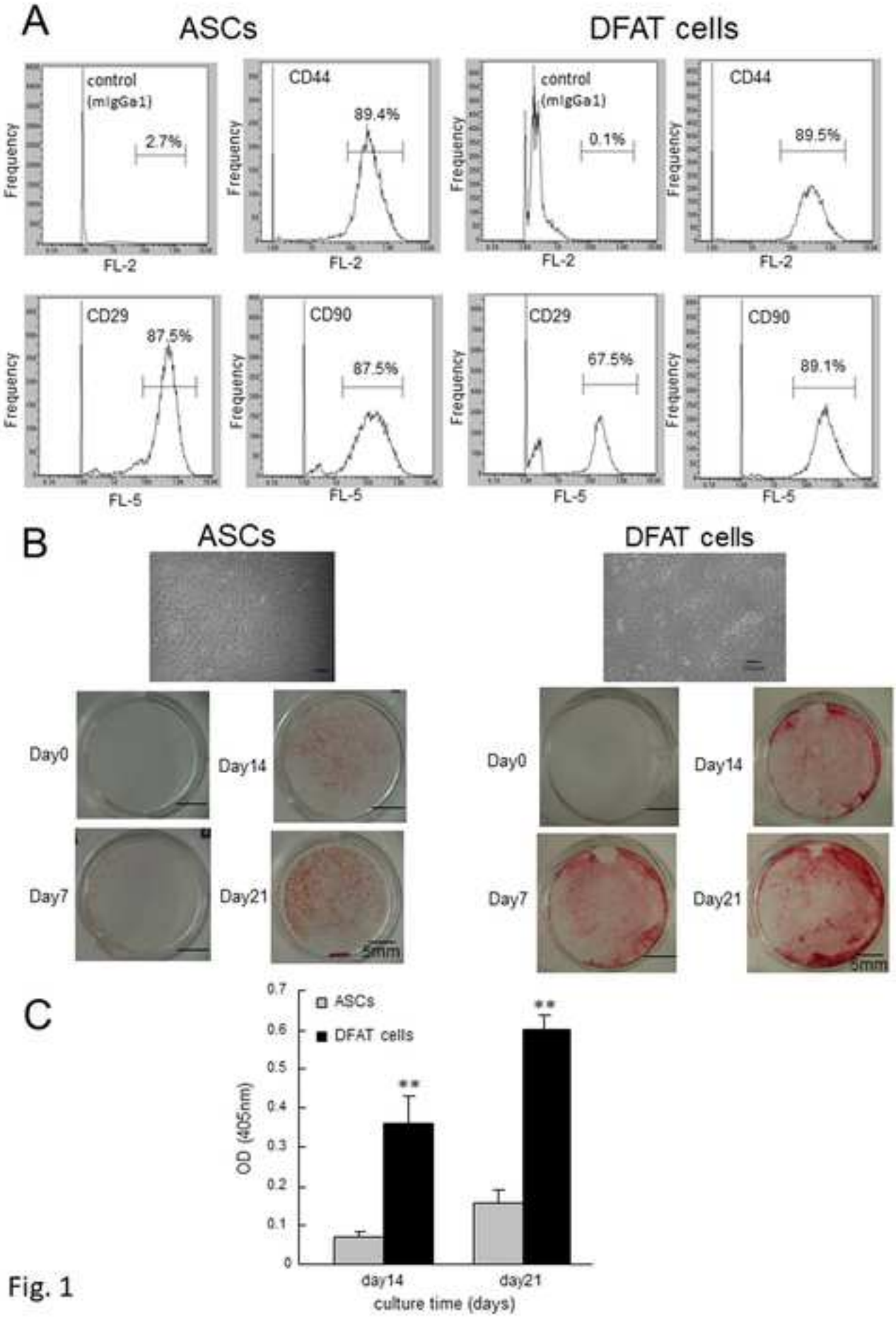

Fig. 1

Figure2

Click here to access/download;Figure;Fig2h(300).tif

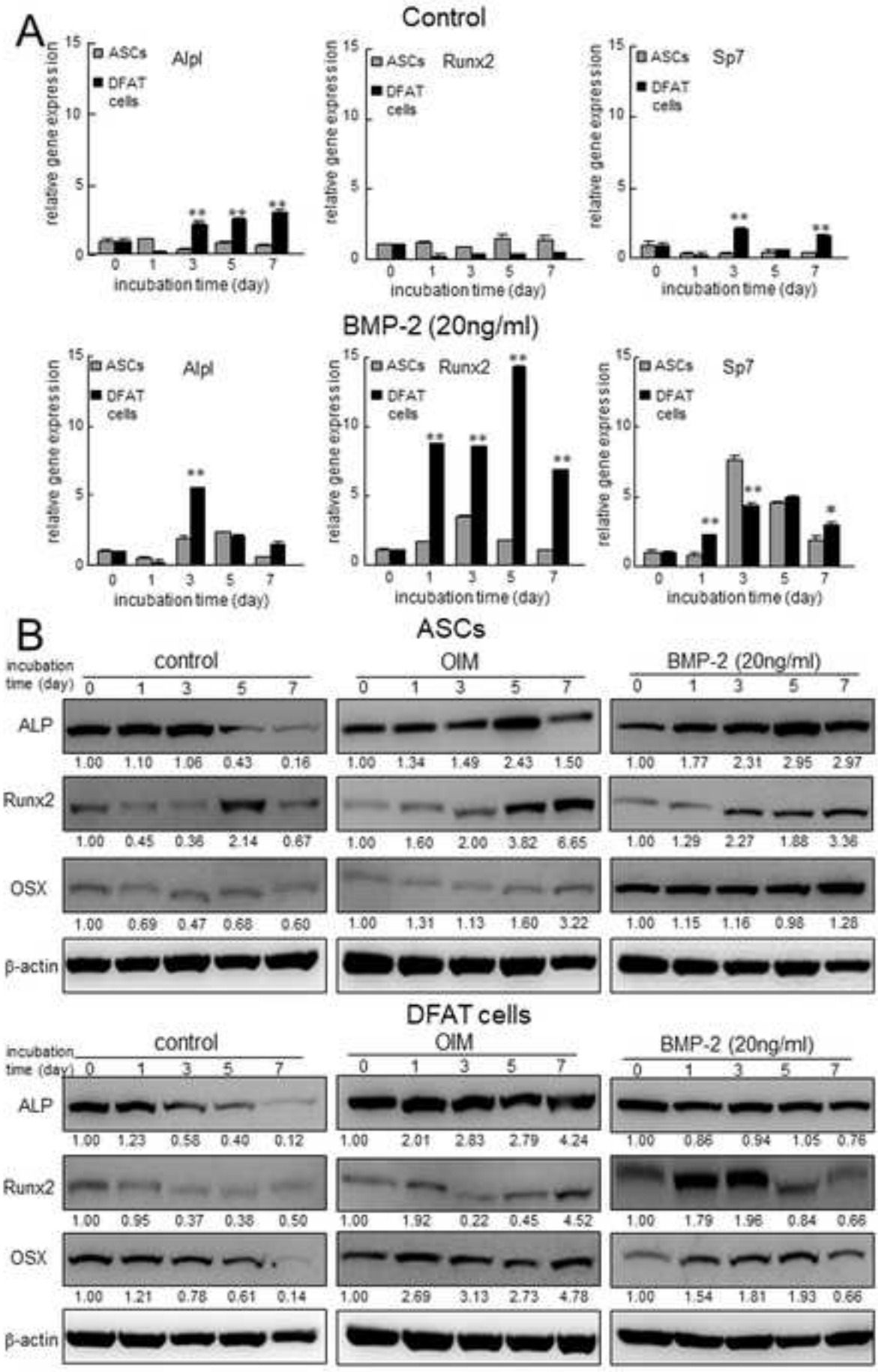

Fig. 2

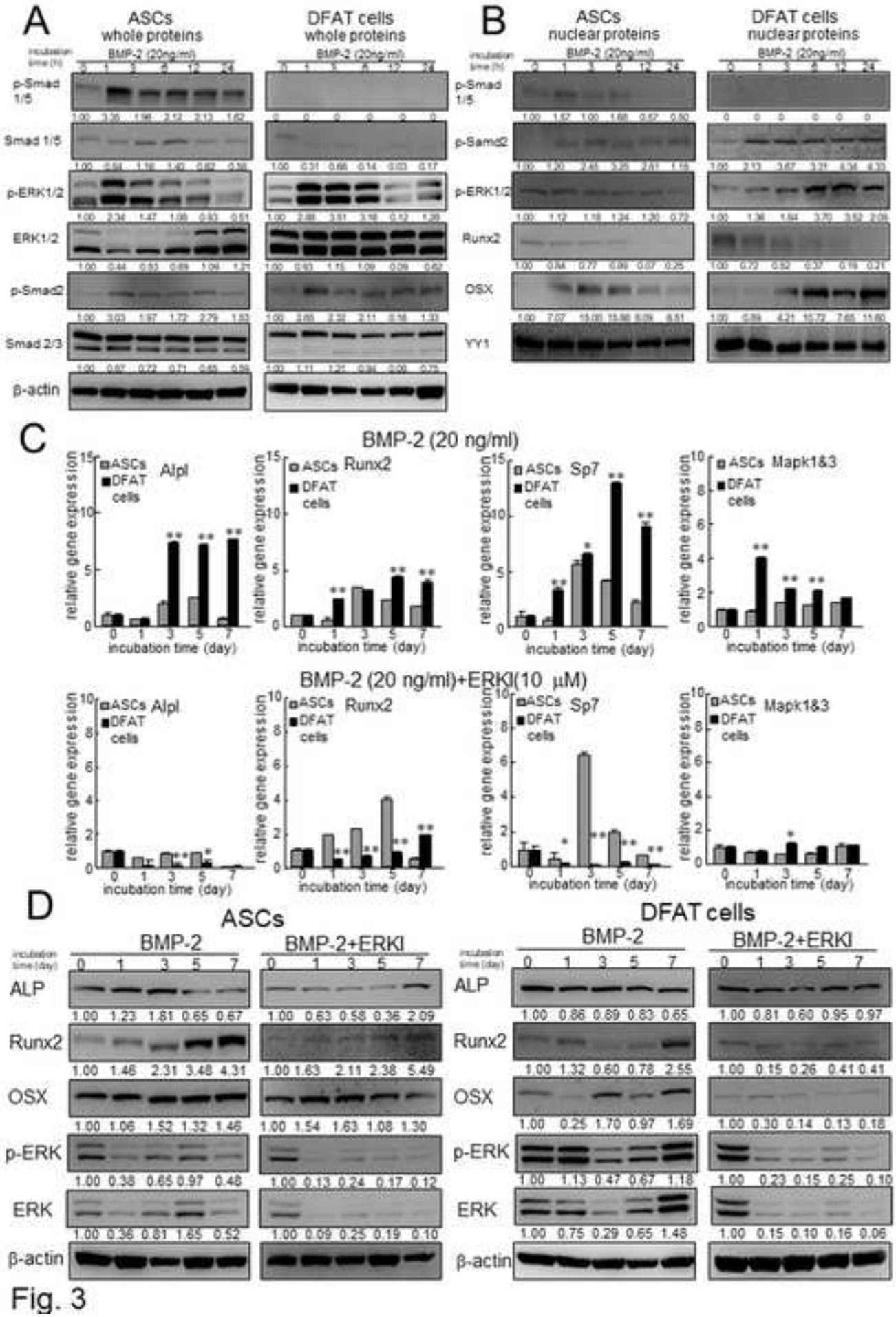

Fig. 3

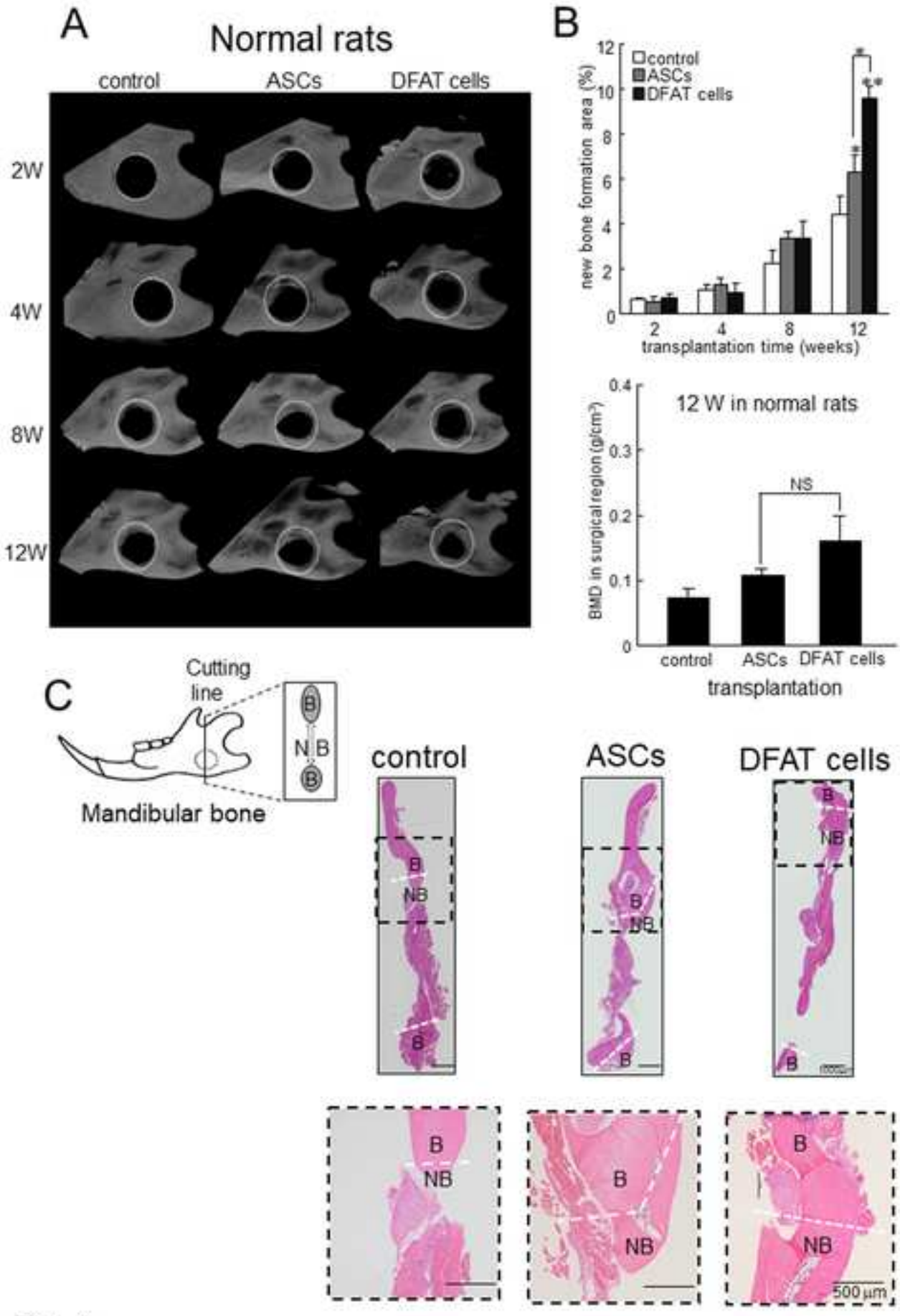

Fig. 4

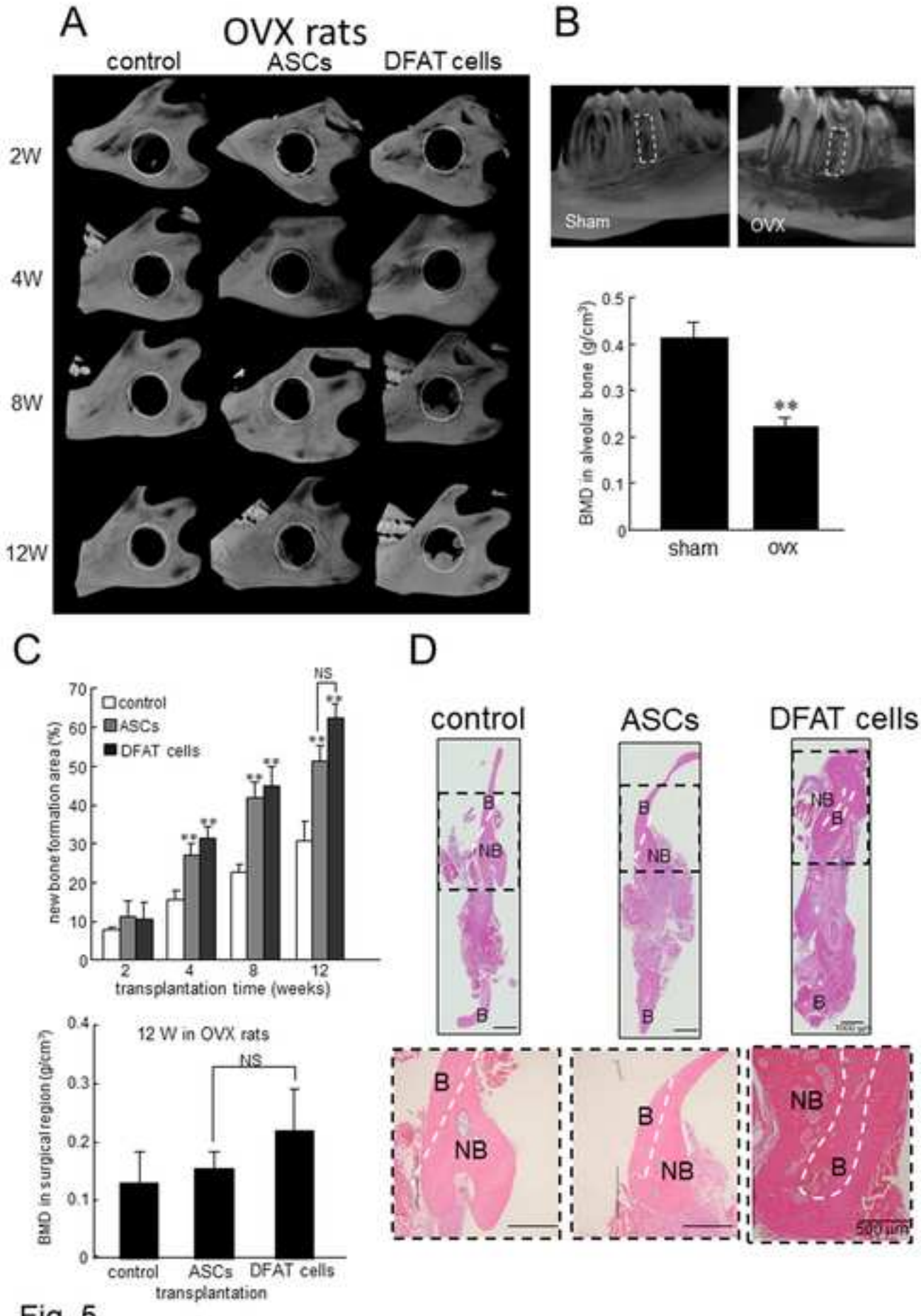

Fig. 5